

Zero-Shot Point Cloud Registration

Weijie Wang^{1,2} Guofeng Mei² Bin Ren^{1,3} Xiaoshui Huang⁴
 Fabio Poiesi² Luc Van Gool³ Nicu Sebe¹ Bruno Lepri²,

weijie.wang@unitn.it, gmei@fbk.eu,

¹University of Trento, Italy ²Fondazione Bruno Kessler, Italy

³Computer Vision Laboratory, ETH Zurich ⁴Shanghai AI Laboratory, China

Abstract

Learning-based point cloud registration approaches have significantly outperformed their traditional counterparts. However, they typically require extensive training on specific datasets. In this paper, we propose ZeroReg, the first zero-shot point cloud registration approach that eliminates the need for training on point cloud datasets. The cornerstone of ZeroReg is the novel transfer of image features from keypoints to the point cloud, enriched by aggregating information from 3D geometric neighborhoods. Specifically, we extract keypoints and features from 2D image pairs using a frozen pretrained 2D backbone. These features are then projected in 3D, and patches are constructed by searching for neighboring points. We integrate the geometric and visual features of each point using our novel parameter-free geometric decoder. Subsequently, the task of determining correspondences between point clouds is formulated as an optimal transport problem. Extensive evaluations of ZeroReg demonstrate its competitive performance against both traditional and learning-based methods. On benchmarks such as 3DMatch, 3DLoMatch, and ScanNet, ZeroReg achieves impressive Recall Ratios (RR) of over 84%, 46%, and 75%, respectively.

1. Introduction

Point cloud registration (PCR) aims to estimate the rigid transformation between a source and a target point cloud [2]. With the overwhelming development of deep learning, the ability of deep features for point cloud registration outperforms traditional hand-crafted counterparts [19, 33, 52]. As a result, PCR has also been effective in challenging scenarios such as low-overlap [29]. However, these scenarios typically require extensive training on specific datasets.

Learning-based methods can be divided into two categories: supervised and unsupervised methods. Supervised methods utilize the transformation or correspondence

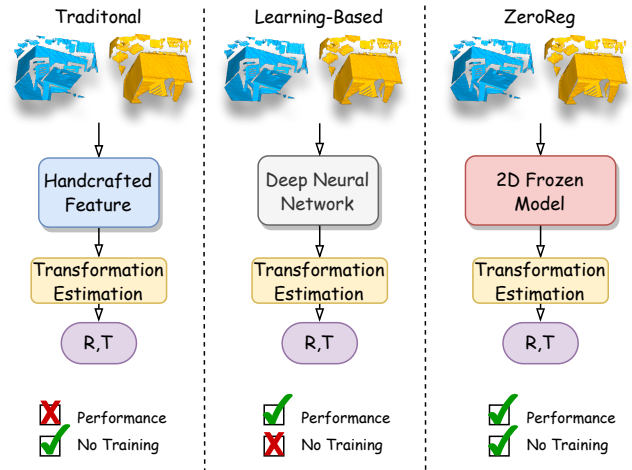


Figure 1. Generally, traditional methods use handcrafted features with high generalization but low performance; learning-based methods achieve high-performance training with the requirements for extensive 3D data. ZeroReg, in contrast, requires no training in 3D data (compared to the learning-based), which utilizes a 2D frozen backbone to achieve higher performance and robust generalization in PCR (compared to the traditional approaches).

annotations as supervision to train neural networks for PCR [12, 18, 26, 39, 40, 56]. Unsupervised methods leverage reconstruction and contrastive learning to train neural networks [16, 22, 32, 41, 47]. Recent unsupervised methods [59] can achieve performance comparable to supervised ones, showing that excellent results can *also* be attained without annotations. Hence, we argue that *point cloud can be aligned with high generalization and accuracy without the requirement for training on point cloud datasets.*

Because RGB and depth information typically come paired, we can use these pieces of information together to assist in PCR based on geometry, which is proving promising [24, 61]. Recent studies have started to explore the image information to establish cross-modal correspondences for PCR tasks [22, 61]. However, most of them primarily in-

corporate 2D semantic features, while ignoring the geometric features between points. Moreover, all of them require extra training, which is costly to deploy in novel scenarios.

In this paper, we propose a simple yet effective zero-shot approach for point cloud registration, which we name ZeroReg. ZeroReg can identify keypoints within 3D point cloud pairs and capture the overlapping regions between them by matching keypoints in 3D space. Given the inherent unordered and irregular nature of point clouds, relying solely on visual features for PCR is inadequate. Thus, the comprehensive integration of geometric information into 2D visual information is non-trivial but promising. Our method combines the visual features from a 2D frozen model with the geometric attributes of point clouds to achieve PCR in a zero-shot manner (Fig. 1).

To achieve this, we first establish the coarse-level correspondences between point cloud pairs from their posed RGB pairs. We adopt SuperPoint [18] to detect the keypoints in images and map these keypoints onto the 3D space. Second, we utilize the 2D frozen model to extract features for the keypoints and utilize optimal transport to establish coarse-level correspondences among the keypoints on the point cloud. Due to the sparsity in the point cloud data, not each pixel can be associated with a corresponding point in 3D space. Thus, to maximize the preservation of keypoints from the images onto the point cloud, we use point clouds reconstructed from depth images with identical poses to the original ones. After obtaining coarse-level keypoints, following [57], we adopt the coarse-to-fine strategy. Then, we apply the K-Nearest-Neighbours algorithm (k NN) [46] to associate keypoints with the neighbouring points, constructing patches. These patches, together with their point-wise visual features extracted from the 2D frozen pretrained backbone, fed into our custom-designed parameter-free decoder to infuse geometric information into visual features, thereby enhancing distinctiveness at the point level. Finally, the task of establishing correspondences between point clouds is formulated as an optimal transport problem, and we use the RANSAC [52] to estimate the transformation. We evaluate ZeroReg on three benchmarks 3DMatch (1.6K pairs) [60], 3DLoMatch (1.7K pairs) [29], ScanNet (26K pairs) [15].

Since our approach is zero-shot, it does not perform on par with the SOTA learning-based approaches with sufficient training data. However, the performance of ZeroReg overall surpasses that of traditional approaches and even competes with some learning-based methods, indicating its potential for pairwise registration tasks. To summarize, our contributions are as follows:

- We propose ZeroReg that, to the best of our knowledge, is the first method that conducts pairwise registration in a zero-shot manner, which eliminates the need for training on the point cloud dataset.

- We design a novel parameter-free geometry decoder that integrates geometric information with visual features for refinement in order to enhance performance. We also demonstrate that the extracted visual features can be utilized for pairwise registration, resulting in improved performance.
- We conduct extensive experiments on three benchmarks such as 3DMatch, 3DLoMatch, and ScanNet, and achieve competitive results, with a Recall Ratio of 84% (3DMatch), 46% (3DLoMatch), and 75% (ScanNet).

2. Related Work

2.1. Learning-based point cloud registration

Based on the input source, current 3D point cloud registration methods can be classified into **single-modal** and **multi-modal**. The former solely relies on the geometry descriptors of the point cloud as input, while the latter utilizes RGB-D images as visual descriptors, or both geometry and visual descriptors complement each other to further enhance point cloud registration performance.

Single-modal. Early point cloud registration methods utilized handcrafted feature extraction e.g., surface normals [19, 33, 52], point coordinates [13], on point cloud geometry for registration [1, 52]. For example, MCOV [13] is a covariance descriptor to directly fuse the texture and shape features in point clouds. PPF [1] and FFPH [52] adopt the geometric features calculated from the distances and relative angles between points and surface normals. With the advancement of deep learning, deep neural networks achieve impressive improvements over handcrafted approaches with training. Most learning-based methods are two-stage methods, which extract rotation-invariant features [16, 17] from point clouds, enabling to estimate feature matching between a pair of sparse points by the Nearest Neighbour Matcher [29, 50, 57, 58], and then adopting the robust transformation estimators, e.g., RANSAC [23], which is still widely applied for registration task. Predator [29] samples keypoints to predict the overlapping regions by incorporating the global context into the local descriptors. Cofinet [57] is a keypoint-free method, which extracts hierarchical correspondences to finish point matching in a coarse-to-fine manner. GeoTrans [50] and RoITr [58] propose the rotation-invariant descriptor using transformers [54]. GeDi [47] proposes a general and distinctive point cloud local descriptor obtained from different domains to conduct registration. Finally, PointNetLK [3] and its variant [30] are single-stage methods, which modify the classic Lucas & Kanade (LK) algorithm and apply it to registration tasks by directly regressing the exact position of points. However, all of the above methods are solely based on the single-source point cloud.

Multi-modal. Compared to single-modal methods, incorporating the visual features from RGB images into geometric features exhibits higher discriminative power [27, 31, 36, 37]. For instance, UR&R [22] employs a differentiable renderer to create projections of point clouds. It then calculates the geometric consistency between these projections and the raw RGB-D video frames for unsupervised point cloud registration. BYOC [20] proposes learning visual and geometric features from RGB-D videos without the need for ground truth pose or correspondence supervision. Based on them, LLT [21] introduces a multi-scale local linear transformation method that integrates visual and geometric features from both RGB and depth images, which mitigate the visual discrepancies resulting from alterations in geometry. PCR-CG [61] designs a 2D-3D module, projecting 2D deep color features into 3D geometry representation. PointMBF [59] implements a multi-scale bidirectional fusion network between RGB images and point clouds, producing more distinctive deep features for correspondence estimation.

However, all existing learning-based methods currently require labor-intensive training, which limits their practical applicability. Handcrafted methods, though not requiring extensive training like deep learning, often struggle with weak performance on challenging cases. In this paper, we present a novel approach that eliminates the requirements for laborious training to conduct point cloud registration.

2.2. Zero-shot learning for 3D point cloud

Zero-shot learning (ZSL) focuses on transferring knowledge from seen categories to unseen categories. Unlike its widespread use in 2D images, the application of ZSL in the 3D domain is limited. Some approaches have employed ZSL to explore classification [8–11] of 3D point clouds. Cheraghian et al. [9] adapt PointNet [48] for object feature extraction while incorporating additional semantic features from W2V [43] or GloVe [45] embeddings to reason the category of unseen objects.

Subsequently, emerging techniques utilize zero-shot learning techniques for the semantic segmentation of 3D point clouds [7, 35, 38, 42]. Some of them [35, 42] utilize a general generative model to produce fake semantic features to achieve the ZSL, with label supervision of the seen class to train. Different from the generative way, TGP [38] learns geometric primitives to transfer knowledge from seen to unseen categories, leveraging visual feature extraction to align with the transductive context. SMKMM [38] utilizes both point clouds and images to align the visual and semantic spaces, enhancing the comprehensive understanding of unseen objects in zero-shot learning.

To our knowledge, none of the ZSL methods is related to point cloud registration. In this paper, we utilize SuperPoint [18] to extract 2D keypoints from images and project

them into their 3D frames. This facilitates coarse-level matching in 3D space, followed by keypoint-to-patch expansion using the K-Nearest-Neighbours (k NN). Lastly, we perform point-level refinement with associated features.

3. Method

In this section, we organize our methodology as follows: Sec. 3.1 outlines the problem formulation. Sec. 3.2 encompasses keypoint detection and feature extraction in the image, where feature extraction is further divided into keypoint descriptors and normal point descriptors. Also, the 2D-3D mapping module and our custom-designed parameter-free decoder are described in this section. Finally, Sec. 3.3 details the correspondence matching part.

3.1. Problem formulation

The pipeline of ZeroReg is illustrated in Fig. 2. Given the point cloud pairs $\mathcal{P} = \{\mathbf{p}_i \in \mathbb{R}^3 | i = 1, 2, \dots, N\}$ and $\mathcal{Q} = \{\mathbf{q}_j \in \mathbb{R}^3 | j = 1, 2, \dots, M\}$, point cloud registration (PCR) aims to calculate the transformation $\mathcal{T} \in SE(3)$ that align the point cloud pairs. Our approach bypasses the direct calculation of \mathcal{T} from point cloud pairs. It utilizes their posed RGB images $\mathcal{I}_{\mathcal{P}} \in \mathbb{R}^{3 \times H \times W}$ and $\mathcal{I}_{\mathcal{Q}} \in \mathbb{R}^{3 \times H \times W}$ to establish correspondences between point cloud pairs in a zero-shot manner.

3.2. Keypoint detection and feature extraction

Keypoint detection. As illustrated in Fig. 2, we utilize Superpoint [18] for keypoint detection of RGB pairs in our default implementation. This part is agnostic and other keypoint algorithms can be implemented using different formulations. For image feature extraction, we chose the ResUNet-50 encoder [28] as the 2D image backbone, which is initialized by a pre-trained model on ImageNet. We extract keypoints and image descriptors for $\mathcal{I}_{\mathcal{P}}$ and $\mathcal{I}_{\mathcal{Q}}$ to obtain keypoint descriptors (denoted as $(\mathcal{F}_{\eta}^{\mathcal{I}_{\mathcal{P}}}, \mathcal{F}_{\eta}^{\mathcal{I}_{\mathcal{Q}}})$) and image descriptors $(\mathcal{F}^{\mathcal{I}_{\mathcal{P}}}, \mathcal{F}^{\mathcal{I}_{\mathcal{Q}}})$

2D-to-3D mapping. To utilize 2D information in the 3D space, it is crucial to establish a mapping bridge between 2D pixels and 3D coordinates. However, due to the sparse nature of point clouds, we chose to utilize the point cloud recovered from the depth image. In theory, point clouds and pixels have a one-to-one correspondence \mathcal{M} , (e.g. $N = H \times W$). Thus, the final projecting process is as Eq. (1):

$$\begin{bmatrix} x_i \\ y_i \\ z_i \end{bmatrix} = [\mathbf{R} | \mathbf{T}] \cdot \left(Z(u, v) \cdot \mathbf{K}^{-1} \cdot \begin{bmatrix} v \\ u \\ 1 \end{bmatrix} \right) \quad (1)$$

where u, v is the depth coordinate corresponding to the i -th point with (x_i, y_i, z_i) 3D coordinate in the point cloud. \mathbf{K} is the intrinsic of the camera, $Z(u, v)$ is the value of depth in the position of (u, v) , \mathbf{R} and \mathbf{T} are the transformation of

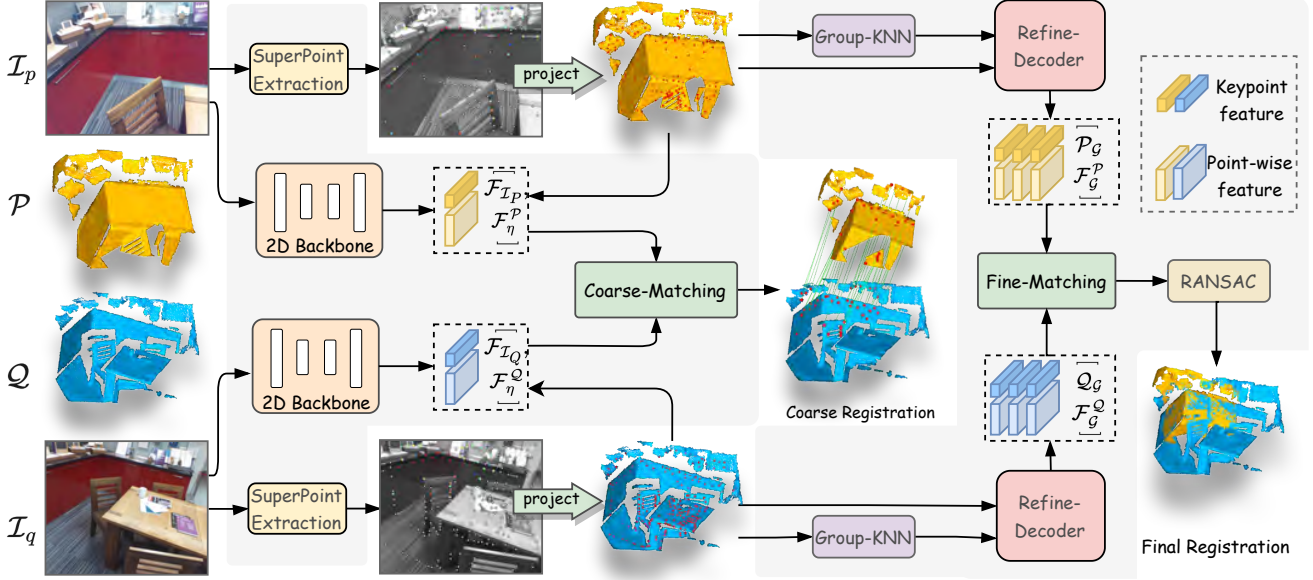


Figure 2. *The pipeline of ZeroReg.* First, extract keypoints from 2D images and project them onto 3D point clouds. Use a 2D image backbone to extract pixel-level features and project them onto point-wise features. Perform coarse-level matching using keypoint features and coordinates. Apply k NN to group keypoints to patches for refinement. Employ a parameter-free decoder to integrate geometric features for refinement in the fine-level matching process. Finally, RANSAC is used to calculate the transformation between the point cloud pairs.

the pose. In practice, various factors, such as inconsistent depths and variations in depth map resolution, contribute to the loss of depth information, resulting in $N < H \times W$. Finally, we obtain the keypoint descriptors (denoted as \mathcal{F}_η^P , \mathcal{F}_η^Q), and point features (\mathcal{F}^P , \mathcal{F}^Q).

Parameter-free decoder for refinement. Depending solely on keypoints, a limited subset of the original point cloud, may not provide enough correspondences for effective registration, particularly in point clouds with low overlap. Additionally, while features transferred from 2D images may miss key geometric details, the inherent geometric structure of point clouds is rich in information.

Motivated by this insight, we develop a parameter-free refinement decoder, which is based on the distance-based propagation strategy [49]. Its primary function is to expand keypoints (\mathcal{F}_η^P , \mathcal{F}_η^Q) in coarse correspondences into patches comprising point groups (\mathcal{P}_G , \mathcal{Q}_G), and their associated descriptors (\mathcal{F}_G^P , \mathcal{F}_G^Q). Our decoder utilizes not only the coordinate information of the points but also the eigenvalue information induced by their surrounding neighbours.

Specifically, we first select L neighbours in Euclidean space for each point, using the k NN algorithm. For each point \mathbf{p}_i , we calculate eigenvalue tuples $\boldsymbol{\lambda}_i = (\lambda_i^1, \lambda_i^2, \lambda_i^3)$ based on the coordinates of L neighbouring points. We then select the K -nearest neighbours from the keypoints in both Euclidean and eigenvalue spaces for each point \mathbf{p}_i .

Let $\{\mathbf{p}_{i_1}, \dots, \mathbf{p}_{i_K}\}$ and $\{\mathbf{f}_{i_1}, \dots, \mathbf{f}_{i_K}\}$ represent the K -nearest neighbours and their corresponding features in Euclidean space, respectively. Similarly, $\{\mathbf{f}_{\bar{i}_1}, \dots, \mathbf{f}_{\bar{i}_K}\}$ and $\{\boldsymbol{\lambda}_{\bar{i}_1}, \dots, \boldsymbol{\lambda}_{\bar{i}_K}\}$ denote the features and eigenvalues of the K -nearest neighbours in eigenvalue space. After that, we implement a reverse distance-weighted average interpolation method, leveraging these neighbours to recover missing point features, denoted as \mathbf{f}_i^c and \mathbf{f}_i^e in Euclidean and eigenvalue spaces, respectively. The interpolation is governed by the following:

$$\begin{aligned} \mathbf{f}_i^c &= \frac{\sum_{k=1}^K w_{i_k}^c(\mathbf{p}_{i_k}) \mathbf{f}_{i_k}}{\sum_{k=1}^K w_{i_k}^c(x)}, w_{i_k}^c(\mathbf{p}_{i_k}) = \frac{1}{\|\mathbf{p}_i, \mathbf{p}_{i_k}\|}, \\ \mathbf{f}_i^e &= \frac{\sum_{k=1}^K w_{i_k}^e(\boldsymbol{\lambda}_{\bar{i}_k}) \mathbf{f}_{\bar{i}_k}}{\sum_{k=1}^K w_{i_k}^e(x)}, w_{i_k}^e(\boldsymbol{\lambda}_{\bar{i}_k}) = \frac{1}{\|\boldsymbol{\lambda}_i, \boldsymbol{\lambda}_{\bar{i}_k}\|}, \end{aligned} \quad (2)$$

where $\|\cdot\|$ is the L_2 norm. Finally, the refined feature \mathbf{f}_i for \mathbf{p}_i is the concatenation of \mathbf{f}_i^c and \mathbf{f}_i^e . This enables us to acquire geometrically enhanced point-level features, which are instrumental in identifying more accurate correspondences for registration purposes.

3.3. Correspondence Prediction

ZeroReg adopts a coarse-to-fine strategy to compute correspondences between points. The rationale is that the global ambiguity is resolved through keypoint matching in the coarse-level stage. Subsequently, in the fine-level stage, the

integration of geometric features into the distance calculation between point pairs enhances point-to-point matching.

Coarse-level correspondence. After obtaining keypoint ($\mathcal{P}_\eta, \mathcal{Q}_\eta$) and corresponding descriptors ($\mathcal{F}_\eta^P, \mathcal{F}_\eta^Q$), we employ a simple yet effective method to compute coarse-level correspondences between them. To enhance optimization stability, we conduct a similarity matrix between $\mathcal{S}_\eta = \Omega(\mathcal{F}_\eta^P, \mathcal{F}_\eta^Q)$, where Ω is the log-space optimal transport [53]. Then, we expand \mathcal{S}_η with a new row and a new column as \mathcal{S}'_η in [6] and calculate it as Eq. (3):

$$\mathcal{S}'_\eta = \begin{bmatrix} \mathcal{F}_\eta^P (\mathcal{F}_\eta^Q)^T & \mathbf{z} \\ \mathbf{z}^T & z \end{bmatrix}, \quad \mathbf{S}' \in \mathbb{R}^{(n'+1) \times (m'+1)} \quad (3)$$

where z is the same learnable parameter. Next, we apply the Sinkhorn Algorithm [14] to \mathcal{S}' , aiming to find an optimal solution for the optimal transport problem. Dropping the last row and last column, the keypoint correspondence \mathcal{C}_η is finally obtained from the optimal process.

Fine-level correspondences. After obtaining the coarse-level correspondences, we apply group- k NN to each matched keypoints to extend groups of points ($\mathcal{P}_G, \mathcal{Q}_G$) and associated grouped descriptors ($\mathcal{F}_G^P, \mathcal{F}_G^Q$). This process identifies their nearest points, subsequently forming patches. Based on patches from coarse correspondences, following [50], we calculate the fine-level correspondences as $\mathcal{C} = \bigcup_{i=1}^{N_G} \mathcal{C}_{\eta_i}$. N_G is the number of patches. Finally, RANSAC [52] can directly compute the transformation with fine-level correspondences for registration.

4. Experiments

In this section, our experiments are organized as follows. First, we detail the experimental setup, including datasets, implementation, and evaluation metrics in Sec. 4.1. To evaluate the effectiveness of different methods, we utilize three benchmarks in our experiments, *3DMatch* and *3DLoMatch* benchmark in Sec. 4.2, *ScanNet* benchmark in Sec. 4.3. Finally, the ablation studies in Sec. 4.4.

4.1. Experiments Setup

Dataset. (1) *3DMatch* and *3DLoMatch* datasets [60], an indoor dataset containing 62 scenes among which 46/8/8 scenes are used for training/validation/testing, respectively. We focus solely on the test data, which comprises 1623 point cloud fragments (from *3DMatch*) and 1781 point cloud fragments (from *3DLoMatch*) and their transformation matrix, preprocessed by [29]. Their overlapping regions exceed 30% and range from 10% to 30%, respectively. (2) *ScanNet-v1* [15] comprises 1045/156/312 scenes for training, validation, and testing, respectively. We generate view pairs in the test set by selecting image pairs with a 20-frame interval, resulting in 26K pairs.

Implementation. ZeroReg is implemented in PyTorch [44] and Open3D [63]. For testing, we use RANSAC with Open3D implementation to estimate transformation between point clouds. All the experiments are conducted on a single Tesla V100 GPU. We resize RGB images at 320×240 . *Coarse-Matching:* For the SuperPoint [18], we employ the Keypoint Threshold $\eta=0.005$, and the Max Keypoints $\alpha = 1024$. *Fine-Matching:* We set the point limit $\beta=64$ for the limit of neighbouring points. In the optimal transport part, we utilize the Sinkhorn algorithm [14], iterating 20 times for matching.

Evaluation metrics. Following the [57], we evaluate the results on several metrics. (1) *Registration Recall (RR):* Measures the percentage of successful pairwise registrations whose error transformation estimated by RANSAC is smaller than a certain threshold, e.g., RMSE < 20cm, compared to ground truth. (2) *Inlier Ratio (IR)* is the ratio of correspondences whose residual error in the geometric space is below a defined threshold of $\sigma = 10cm$, based on the ground truth transformation. (3) *Rotation Error (RE)*, and (4) *Translation Error (TE)*, the computation of average TE and RE is limited to these successfully registered pairs, as failed registrations can yield poses that deviate significantly from the ground truth, rendering the error metrics unreliable. See more details in the supplementary material.

4.2. Performance on 3DMatch and 3DLoMatch

Our competitors on *3DMatch* & *3DLoMatch* can be categorized into two categories. **Traditional:** FGR [62], SM [34], RANSAC [52]. We employ FPFH [52] descriptors of point cloud pairs. PointDSC [5] is an outlier removal method, we put it into the traditional methods part for comparative analysis. **Learning-Based:** 3DSN [25], FCGF [12], D3Feat [4], SpinNet [2], Predator [29], CoFiNet [57], YOHO [55].

4.2.1 Traditional methods comparison

Since traditional methods also do not require training, to ensure that ZeroReg is meaningful, it must outperform traditional handcrafted descriptors (e.g., FPFH) in terms of performance. Thus, we first compare ZeroReg with traditional methods. Following [5], we align 5cm-voxel-downsampled and extract their FPFH descriptor with Open3D. As indicated in Tab. 1, ZeroReg attains the highest *RR* on *3DMatch* and *3DLoMatch*, as well as competitive *RE* and *TE*. ZeroReg exhibits stronger generalization than traditional methods on novel scenes, especially on *3DLoMatch*.

Quantative and quality analysis. On *3DMatch*, PointDSC achieves the best *RE* and *TE*, demonstrating its better registration precision. ZeroReg attains competitive results in both *RE* and *TE* when compared with ‘‘RANSAC-100k ICP’’ since it also incorporates RANSAC to compute the final transformation. Nonetheless, concerning *Registration Recall*, ZeroReg significantly outperforms both PointDSC

Table 1. Quantitative results on 3DMatch and 3DLoMatch, compared with methods using handcrafted FPFH descriptors: best performances are in bold, second-best underlined.

Method(FPFH)	3DMatch			3DLoMatch		
	RE↓	TE↓	RR(%)↑	RE↓	TE↓	RR(%)↑
FGR [62]	4.08	9.83	39.32	5.43	10.44	23.42
SM [34]	2.94	8.15	52.92	6.10	13.00	6.79
RANSAC-1k [52]	5.16	13.65	38.25	4.20	16.17	4.20
RANSAC-10k [52]	4.35	11.79	57.43	7.13	15.04	11.50
RANSAC-100k [52]	3.55	10.04	71.57	6.10	13.94	21.48
RANSAC-100k+ICP[51]	2.62	<u>7.42</u>	74.23	<u>3.54</u>	10.07	<u>28.80</u>
PointDSC [5]	2.07	6.57	<u>75.50</u>	4.37	10.61	27.74
ZeroReg	<u>2.19</u>	7.75	84.41	3.31	10.78	46.43

and “RANSAC-100k ICP” by 8.91% and 10.18% respectively on 3DMatch. We also provide the visualization as Fig. 3 shows. On 3DLoMatch, all the methods exhibit a decrease in three metrics. Both “RANSAC-Based” and PointDSC experience significant performance drops, which proves unsuitable for extremely low-overlap scenarios. The main reason is these methods of sampling interest points within FPFH descriptors, which are scattered globally throughout the entire point cloud. In low-overlap cases, there is a limited number of interest points sampled, resulting in substantial outliers and a drop in performance.

It is noteworthy that the reduction in *Registration Recall* for PointDSC, at 63.25%, is more substantial than that of RANSAC, which stands at 61.20%. It seems like PointDSC is overfitting on 3DMatch. In contrast, ZeroReg demonstrates a 40.27% decrease from 3DMatch to 3DLoMatch, surpassing the second position (RANSAC ICP) by 16.21%. This reduction of 44.99% indicates its superior robustness in low-overlap scenarios. In such cases, RANSAC exhibits inferior performance, as shown in Fig. 4. Quantitative and qualitative analyses reveal that ZeroReg exhibits better robust generalization to novel scenes compared to traditional methods.

Why ZeroReg achieves high RR? As noted by [57], directly detecting keypoints on the point cloud is suboptimal, the strategy of ZeroReg avoid directly doing it. In contrast, ZeroReg detects keypoints across the 2D image pairs and projects them on 3D point cloud pairs as 3D keypoints. One immediate benefit is the utilization of more robust visual features to distinguish, thereby obtaining more reliable keypoints on point cloud pairs. Moreover, the number of keypoints, a pivotal factor in successful pairwise registration, is positively correlated with image size (See Tab. 5). As Fig. 5 shows, even in 3DLoMatch, there is a substantial number of keypoints persist in the source and target pairs (row 1-3). In low-overlap cases, an increased number of keypoints enhances the probability of successful matches, thereby enhancing the *Registration Rate*. Nevertheless, in such circumstances, relying solely on a limited number of key points for matching is unreliable. As shown red box

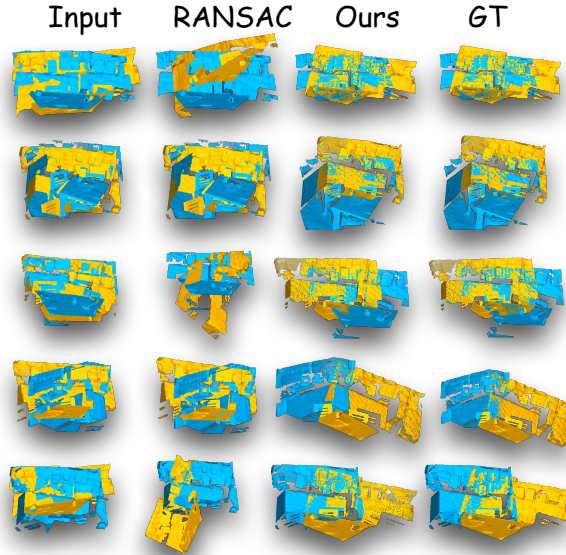


Figure 3. Registration visualization results on 3DMatch.

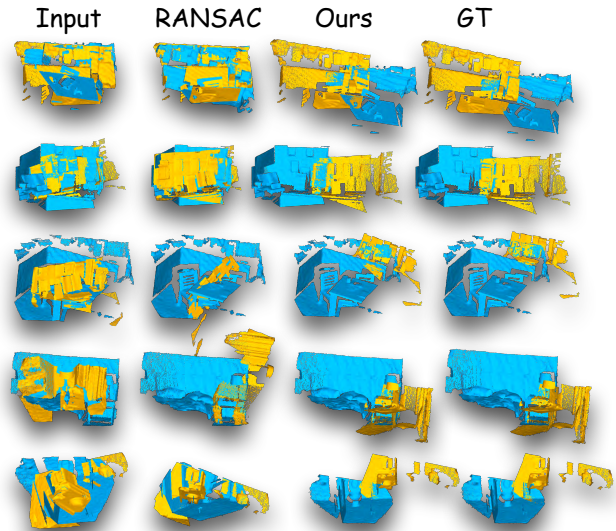


Figure 4. Registration visualization results on 3DLoMatch.

in Fig. 5, there are an exceedingly limited number of keypoints. And these keypoints are mismatched, leading to failure cases (row 4). Also, in extremely low-overlap cases, registration can fail when no keypoints are present on the point cloud, i.e., row 5.

4.2.2 Learning-Based Methods Comparison

As ZeroReg does not need additional training, it is not necessary to perform on par with the SOTA learning-based approaches. However, given the premise of known ZeroReg’s

Table 2. Quantitative results on 3DMatch & 3DLoMatch with a different number of sampling points. Best performance is highlighted in bold while the second best is marked with an underline.

# Samples	3DMatch					3DLoMatch				
	5000	2500	1000	500	250	5000	2500	1000	500	250
<i>Registration Recall (%)</i> ↑										
3DSN [25]	78.4	76.2	71.4	67.6	50.8	33.0	29.0	23.3	17.0	11.0
FCGF [12]	85.1	84.7	83.3	81.6	71.4	40.1	41.7	38.2	35.4	26.8
D3Feat [4]	81.6	84.5	83.4	82.4	77.9	37.2	42.7	46.9	43.8	39.1
SpinNet [2]	88.8	88.0	84.5	79.0	69.2	58.2	56.7	49.8	41.0	26.7
Predator [29]	89.0	89.9	90.6	88.5	86.6	59.8	61.2	62.4	60.8	<u>58.1</u>
CoFiNet [57]	<u>89.3</u>	88.9	88.4	87.4	87.0	67.5	66.2	64.2	63.1	61.0
YOHO [55]	90.8	90.3	<u>89.1</u>	88.6	84.5	<u>65.2</u>	<u>65.5</u>	<u>63.2</u>	56.5	48.0
ZeroReg	84.2	83.6	84.2	84.4	83.8	46.0	46.3	46.2	46.4	46.3
<i>Inlier Ratio (%)</i>										
3DSN [25]	36.0	32.5	26.4	21.5	16.4	11.4	10.1	8.0	6.4	4.8
FCGF [12]	56.8	54.1	48.7	42.5	34.1	21.4	20.0	17.2	14.8	11.6
D3Feat [4]	39.0	38.8	40.4	41.5	41.8	13.2	13.1	14.0	14.6	15.0
SpinNet [2]	48.5	46.2	40.8	35.1	29.0	25.7	23.7	20.6	18.2	13.1
Predator [29]	<u>58.0</u>	<u>58.4</u>	57.1	54.1	49.3	26.7	28.1	28.3	27.5	<u>25.8</u>
CoFiNet [57]	49.8	51.2	51.9	52.2	<u>52.2</u>	24.4	25.9	26.7	26.8	26.9
YOHO [55]	64.4	60.7	<u>55.7</u>	46.4	<u>41.2</u>	25.9	23.3	22.6	18.2	15.0
ZeroReg	52.5	52.6	52.7	<u>53.1</u>	52.9	24.6	24.9	25.0	24.9	25.1

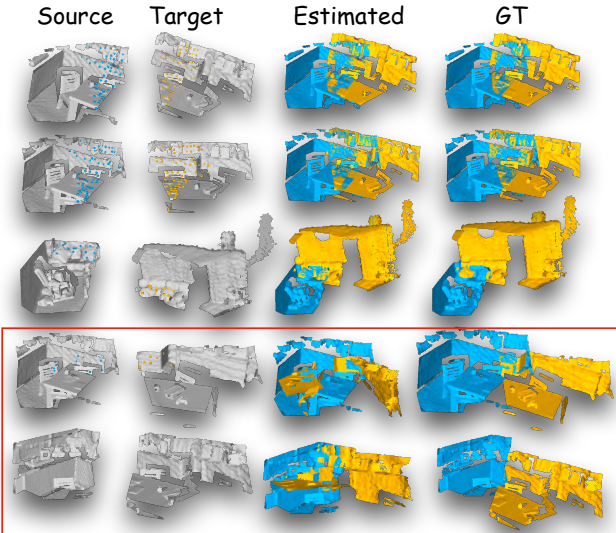


Figure 5. Keypoints visualization and registration results. The red box shows the failure cases.

generalization, it is necessary to evaluate the upper limit of its performance compared to learning-based methods. We assess the performance ceiling of ZeroReg with learning-based methods. For a more comprehensive evaluation, we follow [57] and report performance with different numbers of sampled interest points in terms of RR and IR . ZeroReg overall exceeds 3DSN, FCGF, and D3Feat by a large margin on 3DMatch and 3DLoMatch, which indicates the potential to PCR in a zero-shot manner.

Table 3. Quantitative results on ScanNet with traditional methods with FPFH descriptors. Best performance is highlighted in bold while the second best is marked with an underline.

Method	RE ↓	TE ↓	RR [%] ↑
FGR [62]	5.95	11.78	41.42
SM [34]	<u>3.94</u>	<u>11.14</u>	57.06
RANSAC-1k [52]	5.11	12.85	55.91
RANSAC-10k [52]	4.60	12.09	58.65
RANSAC-100k [52]	4.42	11.89	59.06
RANSAC-100k ICP [51]	3.22	10.66	<u>59.90</u>
PointDSC [5]	4.14	11.51	59.39
ZeroReg	4.17	11.65	75.13

Registration recall. It is worth mentioning that, in addition to FPFH, our method consistently outperforms learning-based descriptors trained on 3DMatch, such as FCGF, in most settings. Exceptionally good results are achieved in all scenarios except when the sample point is set to 5000 and 2500. ZeroReg achieves performance situated between that of SpinNet and Predator in terms of RR on 3DMatch and 3DLoMatch. In the case of “ $Sample=250$ & $=500$ ”, we surpass SpinNet on both benchmarks. Moreover, we even compete with YOHO when “ $Sample=250$ ”. As the decrease of “ $Sample$ ”, the performance of all learning-based methods exhibits a downward trend, while ZeroReg’s performance remains stable overall, displaying minimal performance fluctuation. It indicates that ZeroReg is not sensitive to the sampling point number. Moreover, keypoints exhibit strong discriminativeness in contrast to other ordinary points, irrespective of the quantity of sampling points. Thus, in the case of a low sampling point, ZeroReg is more promising.

Inlier ratio. ZeroReg achieves significant performance in terms of selecting inlier. As Tab. 2, most learning-based methods decrease performance with fewer sampled points. They require substantial sampling points for optimal results, while ZeroReg holds the most stable performance in terms of IR as well as RR . The variance of RR/IR is only 0.08/0.04 on 3DMatch and 0.01/0.02 on 3DLoMatch. Whereas, the most stable learning-based method, CoFiNet’s variance is 0.80/5.38 on 3DMatch and 0.82/0.88 on 3DLoMatch. The capability of ZeroReg to occupy inliers can be attributed to the high confidence in the selection of keypoints. Even with an abundance of sampled points, key points consistently remain included. Similar to the RR aspect, YoLo demonstrates sensitivity to sampled points, suffering from a drastic decline, especially on 3DLoMatch.

4.3. Performance on ScanNet

For a comprehensive evaluation, we evaluate ZeroReg on ScanNet, which is a high-overlap dataset with 20-frame intervals but, in terms of quantity, has 26K pairs that are sufficient to evaluate the performance of algorithms com-

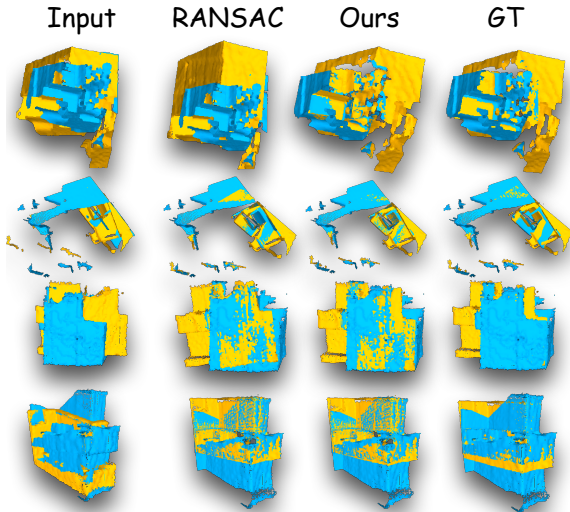


Figure 6. Registration visualization results on ScanNet.

pared to 3DMatch and 3DLoMatch. Our competitors focus on traditional methods. As indicated in Tab. 3, the ZeroReg achieves the highest *registration recall* with a score of 75.13%, surpassing the second-best “RANSAC-100k ICP” of 59.90%. This illustrates the strong generalization and robustness of ZeroReg, indicating that it can effectively perform registration in most cases, even in novel scenes. Fig. 6 is visualization results. In terms of *RE* and *TE*, “RANSAC-100k ICP” achieves the best, attributed to the refinement by ICP, resulting in higher registration accuracy. PointDSC suffers from significant drops on ScanNet compared to 3DMatch. The reason for the decline is that PointDSC conducted training on 3DMatch, the low generalization performance on ScanNet, similar to 3DLoMatch.

4.4. Ablation studies

In this section, we conduct ablation studies on the main components of ZeroReg, i.e., keypoint detection and feature refinement decoder, as well as the impact of image size on 3DMatch and 3DLoMatch.

Keypoint detection and decoder for refinement. Tab. 4 demonstrates the impact of these two main modules on the registration performance. As can be seen, using either of these two modules (*KP* and *Decoder*) leads to substantial *RR* and *IR*, and using both yields the best results. In summary, omitting the *KP* part would significantly decrease the model’s performance, as evidenced by decreased *RR* on 3DMatch and 3DLoMatch. *KP* is crucial for successful pairwise registration. Utilizing the *Parameter-free Decoder* module for feature refinement would further boost performance, owing to the integration of geometric features on the basis of visual features. Overall, ZeroReg achieves its best results when both keypoint detection and feature re-

Table 4. The impact of the keypoint detection and feature refinement decoder on different metrics of ZeroReg (“Samples=500”).

# Samples=500	3DMatch		
	Module	<i>RE</i> ↓	<i>TE</i> ↓
w/o KP	2.53	8.23	75.23
w/o Decoder	2.18	7.80	82.99
ZeroReg	2.19	7.75	84.40
# Samples=500	3DLoMatch		
	Module	<i>RE</i> ↓	<i>TE</i> ↓
w/o KP	5.98	12.32	29.23
w/o Decoder	3.44	11.12	44.24
ZeroReg	3.37	10.78	46.40

Table 5. Ablation studies on Image Size, *2D Keypoint* denotes the quantity of keypoint in image.

ImageSize	3DMatch			<i>2D Keypoint</i>	Time(s) ↓
	<i>RE</i> ↓	<i>TE</i> ↓	<i>RR</i> [%] ↑		
Smaller	2.18	7.80	82.99	200 ± 50	3.1
Larger	2.18	7.78	84.66	400 ± 50	11.2
ImageSize	3DLoMatch			<i>Keypoint</i>	Time(s) ↓
	<i>TE</i> ↓	<i>RE</i> ↓	<i>RR</i> [%] ↑		
Smaller	11.31	3.31	44.58	200 ± 50	3.1
Larger	11.04	3.32	49.07	400 ± 50	11.2

finement are utilized, demonstrating their synergistic effect in enhancing pairwise registration.

Image size. The image size impacts the number of keypoints, thereby affecting the number of matched pairs in both the coarse and refined stages as Tab. 5 shows. We remove the decoder part to verify the impact of image size on the keypoint number. We compared two settings: 320×240 and 640×480. It demonstrates that changing the image size notably improves *RR* and the quantity of keypoints. As the image size increases, the number of pixels increases accordingly. Consequently, the number of keypoints also increases. This results in a significant number of potential correspondences that can be successfully matched within the point cloud pairs. However, the larger size(640×480) results in longer processing times, which is approximately 3.2 times longer to process than the smaller size(320×240). It is a trade-off between efficiency and performance.

5. Conclusion

In this paper, we propose ZeroReg a novel zero-shot pairwise registration method, which does not require training on point cloud datasets. Our approach utilizes an existing 2D visual backbone to directly search for reliable keypoints on 3D point cloud pairs and effectively capture overlapping regions. Additionally, we custom-designed a parameter-free decoder for feature refinement to integrate 2D visual features and geometric information. The fusion of features

would exhibit distinctiveness during matching, further enhancing performance in pairwise registration. Extensive experiments on different benchmarks show that our method not only surpasses traditional approaches but also competes favorably with learning-based methods. Our method expands upon existing traditional and learning-based approaches, which suggests a new potential research direction for pairwise direction.

References

- [1] Dror Aiger, Niloy J Mitra, and Daniel Cohen-Or. 4-points congruent sets for robust pairwise surface registration. In *ACM SIGGRAPH 2008 papers*, pages 1–10. 2008. [2](#)
- [2] Sheng Ao, Qingyong Hu, Bo Yang, Andrew Markham, and Yulan Guo. Spinnet: Learning a general surface descriptor for 3d point cloud registration. In *CVPR*, 2021. [1](#), [5](#), [7](#)
- [3] Yasuhiro Aoki, Hunter Goforth, Rangaprasad Arun Srivatsan, and Simon Lucey. Pointnetlk: Robust & efficient point cloud registration using pointnet. In *CVPR*, pages 7163–7172, 2019. [2](#)
- [4] Xuyang Bai, Zixin Luo, Lei Zhou, Hongbo Fu, Long Quan, and Chiew-Lan Tai. D3feat: Joint learning of dense detection and description of 3d local features. In *CVPR*, pages 6359–6367, 2020. [5](#), [7](#)
- [5] Xuyang Bai, Zixin Luo, Lei Zhou, Hongkai Chen, Lei Li, Zeyu Hu, Hongbo Fu, and Chiew-Lan Tai. Pointdsc: Robust point cloud registration using deep spatial consistency. In *CVPR*, pages 15859–15869, 2021. [5](#), [6](#), [7](#)
- [6] Benjamin Busam, Marco Esposito, Simon Che’Rose, Nassir Navab, and Benjamin Frisch. A stereo vision approach for cooperative robotic movement therapy. In *ICCV workshop*, pages 519–527, 2015. [5](#)
- [7] Runnan Chen, Xinge Zhu, Nenglu Chen, Wei Li, Yuexin Ma, Ruigang Yang, and Wenping Wang. Bridging language and geometric primitives for zero-shot point cloud segmentation. In *ACMMM*, pages 5380–5388, 2023. [3](#)
- [8] Ali Cheraghian, Shafin Rahman, Dylan Campbell, and Lars Petersson. Mitigating the hubness problem for zero-shot learning of 3d objects. *BMVC*, 2019. [3](#)
- [9] Ali Cheraghian, Shafin Rahman, and Lars Petersson. Zero-shot learning of 3d point cloud objects. In *MVA*, pages 1–6. IEEE, 2019. [3](#)
- [10] Ali Cheraghian, Shafin Rahman, Dylan Campbell, and Lars Petersson. Transductive zero-shot learning for 3d point cloud classification. In *WACV*, pages 923–933, 2020.
- [11] Ali Cheraghian, Shafin Rahman, Townim F Chowdhury, Dylan Campbell, and Lars Petersson. Zero-shot learning on 3d point cloud objects and beyond. *IJCV*, 130(10):2364–2384, 2022. [3](#)
- [12] Christopher Choy, Jaesik Park, and Vladlen Koltun. Fully convolutional geometric features. In *ICCV*, pages 8958–8966, 2019. [1](#), [5](#), [7](#)
- [13] Pol Cirujeda, Xavier Mateo, Yashin Dicente, and Xavier Binefa. Mcov: a covariance descriptor for fusion of texture and shape features in 3d point clouds. In *3DV*, pages 551–558. IEEE, 2014. [2](#)
- [14] Marco Cuturi. Sinkhorn distances: Lightspeed computation of optimal transport. *Advances in neural information processing systems*, 26, 2013. [5](#)
- [15] Angela Dai, Angel X. Chang, Manolis Savva, Maciej Halber, Thomas Funkhouser, and Matthias Nießner. Scannet: Richly-annotated 3d reconstructions of indoor scenes. In *CVPR*, 2017. [2](#), [5](#)
- [16] Haowen Deng, Tolga Birdal, and Slobodan Ilic. Ppf-foldnet: Unsupervised learning of rotation invariant 3d local descriptors. In *CVPR*, 2018. [1](#), [2](#)
- [17] Haowen Deng, Tolga Birdal, and Slobodan Ilic. Ppfnet: Global context aware local features for robust 3d point matching. In *CVPR*, pages 195–205, 2018. [2](#)
- [18] Daniel DeTone, Tomasz Malisiewicz, and Andrew Rabinovich. Superpoint: Self-supervised interest point detection and description. In *CVPR*, pages 224–236, 2018. [1](#), [2](#), [3](#), [5](#)
- [19] Bertram Drost, Markus Ulrich, Nassir Navab, and Slobodan Ilic. Model globally, match locally: Efficient and robust 3d object recognition. In *CVPR*, pages 998–1005. Ieee, 2010. [1](#), [2](#)
- [20] Mohamed El Banani and Justin Johnson. Bootstrap your own correspondences. In *ICCV*, pages 6433–6442, 2021. [3](#)
- [21] Mohamed El Banani and Justin Johnson. Improving rgb-d point cloud registration by learning multi-scale local linear transformation. In *ECCV*, 2022. [3](#)
- [22] Mohamed El Banani, Luya Gao, and Justin Johnson. Unsuperviseddr&r: Unsupervised point cloud registration via differentiable rendering. In *CVPR*, pages 7129–7139, 2021. [1](#), [3](#)
- [23] Martin A Fischler and Robert C Bolles. Random sample consensus: a paradigm for model fitting with applications to image analysis and automated cartography. *Communications of the ACM*, 24(6):381–395, 1981. [2](#)
- [24] Francesco Giuliari, Geri Skenderi, Marco Cristani, Yiming Wang, and Alessio Del Bue. Spatial commonsense graph for object localisation in partial scenes. In *CVPR*, pages 19518–19527, 2022. [1](#)
- [25] Zan Gojcic, Caifa Zhou, Jan D Wegner, and Andreas Wieser. The perfect match: 3d point cloud matching with smoothed densities. In *CVPR*, pages 5545–5554, 2019. [5](#), [7](#)
- [26] Zan Gojcic, Caifa Zhou, Jan D Wegner, Leonidas J Guibas, and Tolga Birdal. Learning multiview 3d point cloud registration. In *CVPR*, pages 1759–1769, 2020. [1](#)
- [27] Ahmed Hatem, Yiming Qian, and Yang Wang. Point-tta: Test-time adaptation for point cloud registration using multi-task meta-auxiliary learning. In *ICCV*, pages 16494–16504, 2023. [3](#)
- [28] Kaiming He, Xiangyu Zhang, Shaoqing Ren, and Jian Sun. Deep residual learning for image recognition. In *CVPR*, 2016. [3](#)
- [29] Shengyu Huang, Zan Gojcic, Mikhail Usvyatsov, Andreas Wieser, and Konrad Schindler. Predator: Registration of 3d point clouds with low overlap. In *CVPR*, pages 4267–4276, 2021. [1](#), [2](#), [5](#), [7](#)
- [30] Xiaoshui Huang, Guofeng Mei, and Jian Zhang. Feature-metric registration: A fast semi-supervised approach for robust point cloud registration without correspondences. In *CVPR*, pages 11366–11374, 2020. [2](#)

- [31] Xiaoshui Huang, Wentao Qu, Yifan Zuo, Yuming Fang, and Xiaowei Zhao. Imfnet: Interpretable multimodal fusion for point cloud registration. *IEEE Robotics and Automation Letters*, 7(4):12323–12330, 2022. 3
- [32] Eldar Insafutdinov and Alexey Dosovitskiy. Unsupervised learning of shape and pose with differentiable point clouds. *Advances in neural information processing systems*, 31, 2018. 1
- [33] Andrew E Johnson and Martial Hebert. Using spin images for efficient object recognition in cluttered 3d scenes. *IEEE TPAMI*, 21(5):433–449, 1999. 1, 2
- [34] Marius Leordeanu and Martial Hebert. A spectral technique for correspondence problems using pairwise constraints. In *ICCV*, pages 1482–1489, 2005. 5, 6, 7
- [35] Bo Liu, Shuang Deng, Qiulei Dong, and Zhanyi Hu. Language-level semantics conditioned 3d point cloud segmentation. *arXiv preprint arXiv:2107.00430*, 2021. 3
- [36] Jiuming Liu, Guangming Wang, Zhe Liu, Chaokang Jiang, Marc Pollefeys, and Hesheng Wang. Regformer: An efficient projection-aware transformer network for large-scale point cloud registration. In *ICCV*, pages 8451–8460, 2023. 3
- [37] Quan Liu, Hongzi Zhu, Yunsong Zhou, Hongyang Li, Shan Chang, and Minyi Guo. Density-invariant features for distant point cloud registration. In *ICCV*, pages 18215–18225, 2023. 3
- [38] Yuhang Lu, Qi Jiang, Runnan Chen, Yuenan Hou, Xinge Zhu, and Yuexin Ma. See more and know more: Zero-shot point cloud segmentation via multi-modal visual data. In *ICCV*, 2023. 3
- [39] Guofeng Mei, Xiaoshui Huang, Jian Zhang, and Qiang Wu. Overlap-guided coarse-to-fine correspondence prediction for point cloud registration. In *ICME*, pages 1–6, 2022. 1
- [40] Guofeng Mei, Fabio Poiesi, Cristiano Saltori, Jian Zhang, Elisa Ricci, and Nicu Sebe. Overlap-guided gaussian mixture models for point cloud registration. In *WACV*, pages 4511–4520, 2023. 1
- [41] Guofeng Mei, Hao Tang, Xiaoshui Huang, Weijie Wang, Juan Liu, Jian Zhang, Luc Van Gool, and Qiang Wu. Unsupervised deep probabilistic approach for partial point cloud registration. In *CVPR*, pages 13611–13620, 2023. 1
- [42] Björn Michele, Alexandre Boulch, Gilles Puy, Maxime Bucher, and Renaud Marlet. Generative zero-shot learning for semantic segmentation of 3d point clouds. In *3DV*, pages 992–1002. IEEE, 2021. 3
- [43] Tomas Mikolov, Ilya Sutskever, Kai Chen, Greg S Corrado, and Jeff Dean. Distributed representations of words and phrases and their compositionality. *Advances in neural information processing systems*, 26, 2013. 3
- [44] Adam Paszke, Sam Gross, Francisco Massa, Adam Lerer, James Bradbury, Gregory Chanan, Trevor Killeen, Zeming Lin, Natalia Gimelshein, Luca Antiga, et al. Pytorch: An imperative style, high-performance deep learning library. *Advances in neural information processing systems*, 32, 2019. 5
- [45] Jeffrey Pennington, Richard Socher, and Christopher D Manning. Glove: Global vectors for word representation. In *EMNLP*, pages 1532–1543, 2014. 3
- [46] Leif E Peterson. K-nearest neighbor. *Scholarpedia*, 4(2): 1883, 2009. 2
- [47] Fabio Poiesi and Davide Boscaini. Learning general and distinctive 3d local deep descriptors for point cloud registration. In *IEEE TPAMI*, (early access) 2022. 1, 2
- [48] Charles R Qi, Hao Su, Kaichun Mo, and Leonidas J Guibas. Pointnet: Deep learning on point sets for 3d classification and segmentation. In *CVPR*, pages 652–660, 2017. 3
- [49] Charles Ruizhongtai Qi, Li Yi, Hao Su, and Leonidas J Guibas. Pointnet++: Deep hierarchical feature learning on point sets in a metric space. *Advances in neural information processing systems*, 30, 2017. 4
- [50] Zheng Qin, Hao Yu, Changjian Wang, Yulan Guo, Yuxing Peng, Slobodan Ilic, Dewen Hu, and Kai Xu. Geotransformer: Fast and robust point cloud registration with geometric transformer. *IEEE TPAMI*, 2023. 2, 5
- [51] Szymon Rusinkiewicz and Marc Levoy. Efficient variants of the icp algorithm. In *Proceedings third international conference on 3-D digital imaging and modeling*, pages 145–152. IEEE, 2001. 6, 7
- [52] Radu Bogdan Rusu, Nico Blodow, and Michael Beetz. Fast point feature histograms (fpfh) for 3d registration. In *ICRA*, pages 3212–3217. IEEE, 2009. 1, 2, 5, 6, 7
- [53] Paul-Edouard Sarlin, Daniel DeTone, Tomasz Malisiewicz, and Andrew Rabinovich. Superglue: Learning feature matching with graph neural networks. In *CVPR*, pages 4938–4947, 2020. 5
- [54] Ashish Vaswani, Noam Shazeer, Niki Parmar, Jakob Uszkoreit, Llion Jones, Aidan N Gomez, Łukasz Kaiser, and Illia Polosukhin. Attention is all you need. *Advances in neural information processing systems*, 30, 2017. 2
- [55] Haiping Wang, Yuan Liu, Zhen Dong, and Wenping Wang. You only hypothesize once: Point cloud registration with rotation-equivariant descriptors. In *ACM MM*, 2022. 5, 7
- [56] Kwang Moo Yi, Eduard Trulls, Vincent Lepetit, and Pascal Fua. Lift: Learned invariant feature transform. In *ECCV*, pages 467–483. Springer, 2016. 1
- [57] Hao Yu, Fu Li, Mahdi Saleh, Benjamin Busam, and Slobodan Ilic. Cofinet: Reliable coarse-to-fine correspondences for robust point cloud registration. In *Neurips*, 2021. 2, 5, 6, 7
- [58] Hao Yu, Zheng Qin, Ji Hou, Mahdi Saleh, Dongsheng Li, Benjamin Busam, and Slobodan Ilic. Rotation-invariant transformer for point cloud matching. In *CVPR*, 2023. 2
- [59] Mingzhi Yuan, Kexue Fu, Zhihao Li, Yucong Meng, and Manning Wang. Pointmbf: A multi-scale bidirectional fusion network for unsupervised rgb-d point cloud registration. In *ICCV*, 2023. 1, 3
- [60] Andy Zeng, Shuran Song, Matthias Nießner, Matthew Fisher, Jianxiong Xiao, and Thomas Funkhouser. 3dmatch: Learning local geometric descriptors from rgb-d reconstructions. In *CVPR*, pages 1802–1811, 2017. 2, 5
- [61] Yu Zhang, Junle Yu, Xiaolin Huang, Wenhui Zhou, and Ji Hou. Pcr-cg: Point cloud registration via deep explicit color and geometry. In *European Conference on Computer Vision*, pages 443–459. Springer, 2022. 1, 3

- [62] Qian-Yi Zhou, Jaesik Park, and Vladlen Koltun. Fast global registration. In *ECCV*, pages 766–782. Springer, 2016. [5](#), [6](#), [7](#)
- [63] Qian-Yi Zhou, Jaesik Park, and Vladlen Koltun. Open3d: A modern library for 3d data processing. *arXiv preprint arXiv:1801.09847*, 2018. [5](#)